Author's personal copy

Journal of Magnetism and Magnetic Materials 324 (2012) 1698–1705

Contents lists available at SciVerse ScienceDirect

Journal of Magnetism and Magnetic Materials

journal homepage: www.elsevier.com/locate/jmmm

Magnetostatic interactions in cylindrical nanostructures with non-uniform magnetization

O.J. Suarez [a], L.M. Pérez [b], D. Laroze [c,d,*], D. Altbir [e]

[a] Departamento de Física, Universidad Técnica Federico Santa María, Casilla 110-V, Valparaíso, Chile
[b] Departamento de Física y Matemática Aplicada, Universidad de Navarra, 31080 Pamplona, Spain
[c] Max Planck Institute for Polymer Research, D 55021 Mainz, Germany
[d] Instituto de Alta Investigación, Universidad de Tarapacá, Casilla 7D, Arica, Chile
[e] Departamento de Física and Center for the Development of Nanoscience and Nanotechnology, Universidad de Santiago de Chile, Av. Ecuador 3493, Santiago, Chile

ARTICLE INFO

Article history:
Received 21 April 2011
Received in revised form
6 December 2011
Available online 24 December 2011

Keywords:
Magnetic cylindrical nanoparticles
Magnetostatic interaction
Non-uniform magnetization

ABSTRACT

Cylindrical magnetic nanostructures, like nanowires or nanotubes, should be used for the new generation of magnetic devices. Therefore, the investigation of inter-element interaction is an intense area of research. In this paper we investigated cylindrical nanostructures with non-uniform magnetization field. We focus on particles with a periodic magnetization function and using Fourier series we reduced the problem to a single integral expression. Analytical expressions for both, the self and the interaction magnetostatic energy, are given. These expressions are used to analyze multisegmented tubes, as a function of the number of segments and the distance between particles.

© 2011 Elsevier B.V. All rights reserved.

1. Introduction

Arrays of cylindrical magnetic particles, such as wires, rings and tubes with particular geometric ordering have been extensively investigated during the last years. Such structures can be tailored to display different stable magnetized states, depending on their geometric details. Besides the scientific interest in the magnetic properties of these systems, there is evidence that they might be used in the production of new magnetic devices or as media for high density magnetic recording. In particular, two dimensional arrays of magnetic nanoparticles have been proposed as candidates for magnetoresistive random access memory (MRAM) devices [1–3]. In addition, because of their geometry these arrays are very attractive for technological applications in areas such as magneto-optics [4,5].

Wire arrays are produced inside a nanoporous alumina membrane, with high quality and controlled geometrical characteristics. Nanoporous alumina membranes with hexagonal ordering have been prepared by a two-step anodisation process [6,7]. Nanopores are formed by a self-assembling process, and the parameters of the first anodization step determine important characteristics of the final array, such as the degree of order of the final pore array and the interpore distance. The magnetic properties of arrays of nanowires are determined mainly by the magnetic nature of individual nanowires, but also by the symmetries of the topological characteristics of the array. In particular, the study of highly ordered arrays of magnetic wires with diameters typically in the range of tens to hundreds of nanometers is a topic of growing interest [8–11]. This is a consequence of the development of experimental techniques that lead to the production of such arrays in a controllable and ordered way [6,7]. The high ordering of the array, together with the magnetic nature of nanowires, gives rise to outstanding cooperative properties of fundamental and technological interest [12]. Bi-stable nanowires are characterized by square-shaped hysteresis loops defined by the abrupt reversal of the magnetization between two stable remanent states [13,14]. In such systems, effects of interparticle interactions are in general complicated by the fact that the dipolar fields depend upon the magnetization state of each element, which in turn depends upon the fields due to adjacent elements. Therefore, the modeling of interacting arrays of nanowires is often subject to strong simplifications, for example, modeling the wire using a one-dimensional modified classical Ising model [14,15]. Zhan et al. [16] used the dipole approximation including additional length correction. Velázquez and Vázquez [17], considered each microwire as a dipole, in such a way that the axial field generated by a microwire is proportional to its magnetization. Nevertheless, the latter model is merely phenomenological since the comparison of experimental results with a strictly dipolar model shows that the interaction in the actual case is more intense. They have also calculated the magnetostatic field and expanded it in multipolar terms [18], showing that the non-dipolar contributions of the field are

* Corresponding author at: Max Planck Institute for Polymer Research, D 55021 Mainz, Germany.
E-mail address: david.laroze@gmail.com (D. Laroze).

0304-8853/$ - see front matter © 2011 Elsevier B.V. All rights reserved.
doi:10.1016/j.jmmm.2011.12.032

Author's personal copy

non-negligible for distances considered in experiments. Recently, the energy of the magnetostatic interaction between two magnetic elements of arbitrary shape was derived within the framework of a Fourier space approach by Beleggia et al. [19,20]. When a uniform magnetization is considered for each wire, studies of magnetostatic interactions in arrays were performed [21,22]. In addition, micromagnetic calculations [23,24] and Monte Carlo simulations [25] have also been developed. Other studies on wires can be found in Refs. [26–30].

The number of studies on magnetic nanotubes has been growing in the last years [31–34] motivating intense research in the field. Nanotubes exhibit a core-free magnetic configuration leading to uniform switching fields, guaranteeing reproducibility [34,35] and due to their low density they can float in solutions making them suitable for applications in biotechnology [31]. Magnetic measurements [33], numerical simulations [34], and analytical calculations [35] on such tubes have identified two main states: an in-plane magnetic ordering, namely, the flux closure vortex state, and a uniform state with all the magnetic moments pointing parallel to the axis of the tube.

In both cases, magnetic wires and tubes, it is possible to prepare multisegmented particles [36], in which magnetic layers alternate with non-magnetic ones. Experimental and theoretical results of these particles can be found in Refs [37–45]. Also, soft and hard magnetic layers can alternate in a stacking way forming particles with a non uniform and periodic magnetization along its axis. In this way, several magnetic configurations can appear, making necessary particular calculations for each case.

In order to avoid multiple calculations, in this paper we present a general expression for the dipolar energy of cylindrically shaped nanostructures with a periodic general magnetization along its axis such that the vector field varies along it. Because of the periodic nature of the magnetization, it can be expanded in Fourier series, leading to a closed expression for the energy in terms of a single integral. We apply our method to interacting identical multisegment particles.

The paper is organized as follows: In Section 2 the theoretical model for two cylindrical magnetic object is presented. In Section 3, our method is applied to an array of multisegment particles. Finally, conclusions are drawn in Section 4.

2. Theoretical model

The description of a nano-object based on the investigation of the behavior of individual magnetic moments becomes numerically prohibitive. Therefore, we adopt a simplified description of the system in which the discrete distribution of magnetic moments is replaced by a continuous one, defined by a function $\mathbf{M}(\mathbf{r})$ such that $\mathbf{M}(\mathbf{r})\delta V$ gives the total magnetic moment within the element of volume δV centered at $\mathbf{r}$. In this framework, the magnetostatic field can be obtained from $\mathbf{H}(\mathbf{r})=-\nabla U(\mathbf{r})$, where $U(\mathbf{r})$ is the scalar magnetostatic potential given by [46]:

$$U(\mathbf{r})=\oint_{S(V)}\frac{\mathbf{M}(\mathbf{r}')\cdot d\mathbf{S}'}{\Gamma|\mathbf{r}-\mathbf{r}'|}-\int_V\frac{\nabla'\cdot\mathbf{M}(\mathbf{r}')}{\Gamma|\mathbf{r}-\mathbf{r}'|}d^3r', \tag{1}$$

where $\Gamma=4\pi/\gamma_B$, γ_B is a constant for the different unit system, being $\gamma_B=1$ in SI unit while $\gamma_B=4\pi$ for the Gaussian unit.

In what follows we investigate the magnetic state of a two particles system, however, our calculations can be directly extended to more particles. The total magnetostatic energy, E_m, of our two particles system can be written in terms of the self-energies, $E^{[i]}_{self}$ that is, the energies of the isolated particles, and the interaction contribution, $E^{[i,j]}_{int}$, corresponding to the dipolar coupling between them. In general, these terms are

$$E^{[i]}_{self}=-\frac{\mu}{2}\int_{V_i}\mathbf{M}_i(\mathbf{r})\cdot\mathbf{H}_i(\mathbf{r})d^3r \tag{2}$$

and

$$E^{[i,j]}_{int}=-\mu\int_{V_j}\mathbf{M}_j(\mathbf{r})\cdot\mathbf{H}_i(\mathbf{r})d^3r, \tag{3}$$

where μ is a constant for the different unit system, being $\mu=\mu_0=4\pi\times10^{-7}$H/m in SI unit while $\mu=1$ in Gaussian unit. Furthermore, in the dipolar contribution to the self energy an additive term independent of the configuration has been left out [47].

On the other hand, let us consider a general functional dependence of the magnetization field which can be written in general terms, using cylindrical coordinates, as $\mathbf{M}(\mathbf{r})=M_\rho(\rho,\phi,z)\hat\rho+M_\phi(\rho,\phi,z)\hat\phi+M_z(\rho,\phi,z)\hat z$. However, in most cases, the magnetization is geometry dependent, and each component can be described by a separable functional, that means: $M_\xi(\rho,\phi,z)=a_\xi(\rho)b_\xi(\phi)c_\xi(z)$, with $\xi=\{\rho,\phi,z\}$. For example, in nanowires [48–53,21,22] and in nanotubes [35,54] the most typical configurations are the uniform magnetization $\mathbf{M}=M_0\hat z$ and the vortex state $\mathbf{M}=M_\phi(\rho)\hat\phi$. In nanorings [55] a useful model is $\mathbf{M}(\phi)=M_\rho(\phi)\hat\rho+M_\phi(\phi)\hat\phi$, which describes the onion state. Similarly, in nanodots [51]$\mathbf{M}=M_\phi(\rho)\hat\phi+M_z(\rho)\hat z$ has been used. In this expression $M_z=M_0(1-(\rho/\rho_c)^2)^n$ for $0<\rho<\rho_c$ and $M_z=0$ for $\rho>\rho_c$, with ρ_c a parameter related to the core radius and n a non-negative integer. Alternative expressions for M_z have been proposed in the literature [56,57].

2.1. Particular case: two tubes

Let us consider two cylindrical particles of length $2L$, with internal and external radii r_i and R_i, respectively; with $i=1,2$. For simplicity, we assume that they are parallels and that the longitudinal axis of the tube is the z-axis. The relative distance and angle between the tubes is denoted by D_{ij} and by θ, respectively. The basic geometric parameters used in our calculations are summarized in Fig. 1. In what follows we assume that the magnetization is along the z-axis, that is $\mathbf{M}_i(\mathbf{r})=M_{iz}f_i(z)\hat z$. In this case, Eq. (1) for the isolated tubes can be reduced to (see Appendix A):

$$U_i(z,\rho)=\frac{2\pi M_{iz}}{\Gamma}\int_0^\infty d\eta\frac{J_0(\eta\rho)}{\eta}T_i(\eta)g_i(\eta,z), \tag{4}$$

where $T_i(\eta)=R_iJ_1(\eta R_i)-r_iJ_1(\eta r_i)$, whit $J_n(z)$ the Bessel function of the first kind. The last function g_i can be written as $g_i(\eta,z)=g_{iS}(\eta,z)-g_{iV}(\eta,z)$, where g_S and g_V represent the superficial and volumetric contributions:

$$g_{iS}(\eta,z)=\epsilon_i^+\exp(-\eta|z-L|)-\epsilon_i^-\exp(-\eta|z+L|) \tag{5}$$

and

$$g_{iV}(\eta,z)=\int_{-L}^{L}dz'\exp(-\eta|z-z'|)\left[\frac{\partial f_i(z'')}{\partial z''}\right]_{z'}, \tag{6}$$

where $\epsilon_i^\pm=f_i(\pm L)$. If the tube has a uniform magnetization, $f_i(z)=1\forall\mathcal{D}$. In this situation the volumetric contribution to the potential is zero, that is $g_{iV}=0$. On the other hand, the self-energy, given by Eq. (2), can be presented as

$$E^{[i]}_{self}=\frac{\mu M_{iz}}{2}\int_{r_i}^{R_i}d\rho\rho\int_0^{2\pi}d\phi\int_{-L}^{L}dzf_i(z)\left[\frac{\partial U_i(\mathbf{r}_i')}{\partial z'}\right]_z. \tag{7}$$

Since $U_i(\mathbf{r}_i)$ has not dependence on ϕ and the radial integral produces $T_i(\eta)/\eta$ (see Appendix A), the reduced self energy, $e^{[i]}_{self}=E^{[i]}_{self}/\xi_{(i)}$ with $\xi_{(i)}=4\pi\mu M_{iz}^2V_i/\Gamma$, can be written as:

$$e^{[i]}_{self}=\frac{\pi}{2V_i}\int_{-L}^{L}dzf_i(z)\left[\frac{\partial}{\partial z'}\int_0^\infty d\eta\frac{\omega_i(\eta)}{\eta^2}g_i(\eta,z')\right]_z, \tag{8}$$

Author's personal copy

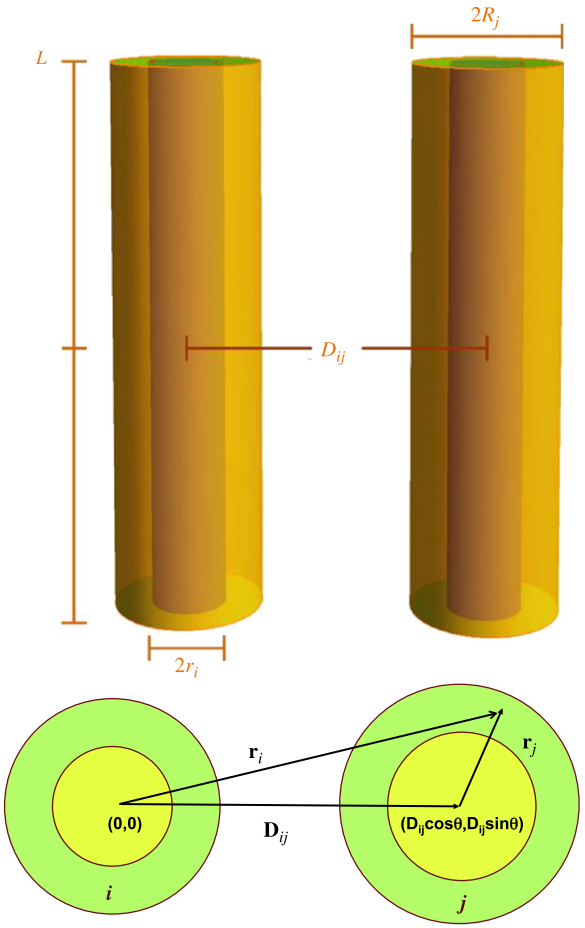


Fig. 1. Schematic representation of a system of two parallel tubes. Both particles have the same length $2L$, but different internal and external radii denoted by r_j and R_j, respectively. (Top) General view of the system. (Bottom) View of a perpendicular plane to the longitudinal tube-axis. The longitudinal axis of the tubes define z-axis. The centers of the tubes are located in $(0,0,0)$ and in $(D_{ij}\cos\theta, D_{ij}\sin\theta, 0)$, respectively.

where $\omega_i(\eta)=(T_i(\eta))^2$. Furthermore, the interaction energy between two particles is given by

$$E_{int}^{[ij]}=\mu M_{jz}\int_{r_j}^{R_j}d\rho\rho\int_0^{2\pi}d\phi\int_{-L}^{L}dzf_j(z)\left[\frac{\partial U_i(\mathbf{r}')}{\partial z'}\right]_z. \tag{9}$$

Using Eq. (4) this expression can be presented as:

$$E_{int}^{[ij]}=\frac{2\pi\mu M_{iz}M_{jz}}{\Gamma}\int_0^{\infty}d\eta\frac{T_i(\eta)}{\eta}\int_0^{2\pi}d\phi \times\int_{-L}^{L}dzf_j(z)\left[\frac{\partial g_i(\eta,z')}{\partial z'}\right]_z\int_{r_j}^{R_j}d\rho\rho J_0(\eta q), \tag{10}$$

where $q=\sqrt{D_{ij}^2+\rho^2+2D_{ij}\rho\cos(\phi-\theta)}$. Using the properties of the Bessel functions [58]:

$$J_0(\Delta)=\sum_{m=-\infty}^{\infty}\exp(im\varphi)J_m(a)J_m(b), \tag{11}$$

with $\Delta^2=a^2+b^2-2ab\cos(\varphi)$. The last expression can be integrated; the angular integral results in $2\pi\delta_{0,m}$ with $\delta_{a,b}$ the Kronecker delta, and consequently the radial integral is $T_j(\eta)/\eta$. Let us define a reduced energy as $e_{int}^{[ij]}=E_{int}^{[ij]}/\xi_{(ij)}$ with $\xi_{(ij)}=4\pi\mu M_{iz}M_{jz}V_j/\Gamma$, hence:

$$e_{int}^{[ij]}=\frac{\pi}{V_i}\int_0^{\infty}d\eta\frac{\omega_{ij}(\eta)}{\eta^2}I_{ij}(\eta), \tag{12}$$

where

$$I_{ij}(\eta)=\int_{-L}^{L}dzf_j(z)\left[\frac{\partial}{\partial z'}g_i(\eta,z')\right]_z \tag{13}$$

with $\omega_{ij}(\eta)=T_i(\eta)T_j(\eta)J_0(D_{ij}\eta)$. We remark that the last expression is the most compact form for the interaction energy for a general $f_j(z)$. When $D_{ij}\to 0$, $J_0(D_{ij}\eta)\to 1$, and the interaction energy reproduces formally the results for the self energy, with the exception of a factor two, which represents the double counting of the self energy.

We are now in position to qualitatively analyze the integrability of both energies. Our main criterion is based on which type of possible functions are non-divergent in the integral with respect to η. With this purpose in mind, we define the *Core* function, $C(\eta,\{\lambda\})$ by $C=\eta^{-2}J_1(a\eta)J_1(b\eta)J_0(D\eta)$ with $\boldsymbol{\lambda}=\{a,b,D\}$. This function always appears in the energy, in fact it is multiplied by different function of η such as $g=1-\exp(-2L\eta)$ [21]. Fig. 2 shows C as a function of η for different values of the parameter D. We can see that in the low η regime, ($\eta\ll 1$), C is approximated by a constant $C\approx C_0(\boldsymbol{\lambda})$, such that C_0 increases when $\{a,b\}$ increases. For the intermediate regime, $O(10^{-2})<\eta<O(10^{1})$, C has an oscillatory behavior. Finally, we see that, regardless of λ, for $\eta>10^1$ the asymptotic value of C is zero, that is $C\sim 0$. Therefore, the core is a smooth function of η, which ensures that the integral will be non-divergent. In the next subsection we will calculate general expressions for the energies when $f_j(z)$ is a periodic function inside the tube.

2.2. Fourier mode expansion

This section is devoted to reduce our expression for the energies, Eqs. (8) and (12), to a single integral problem. Since the magnetization field is null outside the wire, we must define $f_j(z)$ as:

$$f_j(z)=(\Theta(z+L)-\Theta(z-L))\zeta_j(z), \tag{14}$$

where $\Theta(\cdot)$ is the Heaviside distribution and $\zeta_j(z)$ is an arbitrary, but bound function in the range $[-L,L]$. Now, let us assume that $\zeta_j(z)$ is a periodic function. Consequently it can be expanded in Fourier modes:

$$\zeta_j(z)=\sum_{m=-\infty}^{\infty}c_m^{(j)}\exp\left(\frac{im\pi}{L}z\right), \tag{15}$$

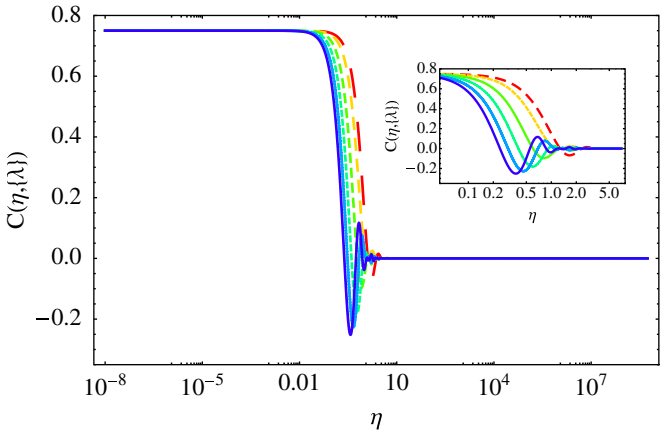


Fig. 2. $C(\eta,\{\lambda\})$ as a function of η for different values of D at $a=1$ and $b=3$. We report results for $D=0$ (red line), 2 (yellow line), 4 (green line), 6 (light green), 8 (light blue) and 10 (blue). (For interpretation of the references to color in this figure legend, the reader is referred to the web version of this article.)

Author's personal copy

where the coefficients $c_m^{(j)}$ are given by

$$c_m^{(j)} = \frac{1}{2L}\int_{-L}^{L} \zeta_j(z)\exp\left(-\frac{im\pi}{L}z\right)dz. \tag{16}$$

Using Eqs. (15) and (16) in Eqs. (8) and (12), one can calculate the integral in $\{z,z'\}$ analytically. Let us write I_{ij} in Eq. (12) in two parts: $I_{ij}=I_{ij}^S+I_{ij}^V$, where the superscripts S and V denotes the superficial and the volumetric part, respectively. Using the Fourier representation for $\zeta_j(z)$ we can evaluate these contributions. The analytical expressions for I_{ij}^S and I_{ij}^V are given by (see Appendix B)

$$I_{ij}^S(\eta) = L\eta\Pi(\eta)\sum_{m=-\infty}^{\infty}\frac{(-1)^m c_m^{(j)}(\epsilon_i^- \alpha_m^* + \epsilon_i^+ \alpha_m)}{|\alpha_m|^2} \tag{17}$$

and

$$I_{ij}^V(\eta) = 2(\pi\eta L)^2\Pi(\eta)\sum_{m,n=-\infty}^{\infty}\frac{(-1)^{m+n} n(m-n)c_m^{(j)}c_n^{(i)}}{|\alpha_m|^2|\alpha_n|^2}, \tag{18}$$

where $\alpha_k=\eta L-i\pi k$ and α_k^* is its complex conjugate, $\epsilon_i^{\pm}=\zeta_i(\pm L)$ and $\Pi(\eta)=1-\exp(-2L\eta)$. Note that Eqs. (17) and (18) are general expressions for any $\zeta_j(z)$. For a specific z-dependence of the magnetization the Fourier coefficients $c_n^{(i)}$ can be calculated. Using Eqs. (8) and (12), both the self and the interaction energy can be obtained through the numerical evaluation of single integrals. In the next section we give an application of this general method.

3. Application

We now apply this approach to the case of magnetic nanostructures consisting of alternate ferromagnetic and nonmagnetic layers arranged within a multilayer structure, called multisegmented magnetic nanostructure. Note that interest in the fabrication and the characterization of this type of structures has increased in the last years due to their possible technological applications [37–43]. In fact, they have been considered as providing the basis for extending magnetic storage densities beyond the superparamagnetic limit. Moreover, in such a system, a single tube with N magnetic layers might store up to 2^N bits, with a volume much larger than those of the grains in conventional recording media, in this way beating thermal fluctuations and increasing the recording density by a factor 2^{N-1} [40,44]. We remark that the phase diagram of these barcode-type nanostructures was recently calculated for different types of magnetic configurations [45], but the interaction between them has not still been reported. Hence, a first study of the interaction between two of these bar-code magnetic structures is in order.

In what follows we consider two identical multisegmented tubes of length $2L$ where the internal and external radii are denoted by r and R, respectively. Let us define the ratio $\beta=r/R$, such that $\beta=0.0$ represents a solid cylinder and $\beta\to1$ corresponds to a slim tube. For both tubes the characterization functions, $\zeta_i(z)=\zeta(z)$, are defined in two branches:

$$\zeta(z)=\begin{cases}\zeta(z^-) & \text{if } z<0,\\ \zeta(z^+) & \text{if } z>0,\end{cases} \tag{19}$$

where

$$\zeta(z^-)=\begin{cases}1, & -L<z<-\upsilon\wedge-\kappa<z<-\iota\\ 0 & \text{other case}\end{cases} \tag{20}$$

and

$$\zeta(z^+)=\begin{cases}1, & \iota<z<\kappa\wedge\upsilon<z<L\\ 0 & \text{other case}\end{cases}, \tag{21}$$

with $\iota=2(k-1)w+d$, $\kappa=2kw-d$, $\upsilon=2\sigma w+d$, $L=Nw$ and being $k=1,\ldots,\sigma$ and $N=2\sigma+1$. Here $\{2d,2(w-d)\}$ denotes the nonmagnetic and magnetic regions, respectively; and N the number of segments, such that $w=L/N$. For these afore mentioned functions the Fourier coefficients, given by Eq. (16), can be written after a straightforward calculation as:

$$c_m=\frac{i\left(e^{imd\pi/L}-e^{im\pi/N}+e^{(im\pi/LN)(2Nd+L)}-e^{(im\pi/NL)(Nd+2L)}\right)}{2m\pi(e^{2im\pi}-1)^{-1}\left(e^{2im\pi/N}-1\right)e^{(im\pi L)(d+L)}}. \tag{22}$$

We remark that for $m=0$ the value of c_0 in Eq. (22) is given by $c_0=1-dN/L$; and that for $m\neq0$ the non-zero values of c_m in Eq. (22) are obtained only when $m=\pm kN$, where k is an integer. For numerical procedures the Fourier series have necessarily to be truncated. Its convergence strongly depends of the number of coefficients that are taken into account, here denoted by P. Also, for functions that have discontinuities, there appears an overshoot (undershoot) in the eigenfunction series, close to the point of discontinuity, called the Gibbs phenomenon [59]. In those cases the inclusion of more and more terms does little to remove the overshoot (undershoot), and only moves it closer to the point of discontinuity. Nevertheless, there is a numerical improvement, called *Lancos $\sigma-$Factor*, that reduces the Gibbs phenomenon [60].

Since the multisegmented structures are modeled by functions with discontinuities, we use this method. The *$\sigma-$approximation* of the Fourier series representation is given by

$$\zeta(z)\approx\sum_{m=-1-P}^{P+1}\tilde{c}_m\exp\left(\frac{im\pi}{L}z\right), \tag{23}$$

where $\tilde{c}_m=\mathrm{sinc}(q_m)c_m$ with $\mathrm{sinc}(x)=\sin(x)/x$ and $q_m=\pi m/(2P)$. For numerical purposes, we chose $L=600$ nm and $d=20$ nm, hence the control parameters to vary are $\{\beta,R,N,D\}$. Fig. 3 shows the periodic function $\zeta(z)$ that describes the multi-segmented tubes as a function of z defined in the interval $-L<z<L$ with $P=200$. We can observe that the amended Fourier expansion, Eq. (23), is in very good agreement with $\zeta(z)$. The numerical value of P has been chosen such that the relative error between $\tilde{c}_m$ and c_m is less than 1%, as shown in Fig. 4. assuring good results in what follows. Now, let us numerically determine the self- and interaction energies using Eqs. (8) and (12), respectively. For convenience, we have scaled the energy axes, $\tilde{e}^i=10^3e_{self}^{[i]}$ and $\tilde{e}^{ij}=10^3e_{int}^{[ij]}$.

3.1. Self energy

In this subsection we explore the dependence of the self-energy, $\tilde{e}^i$, on the tube geometry. Fig. 5 shows $\tilde{e}^i$ as a function of the external radius R for different numbers of segments, N. In this

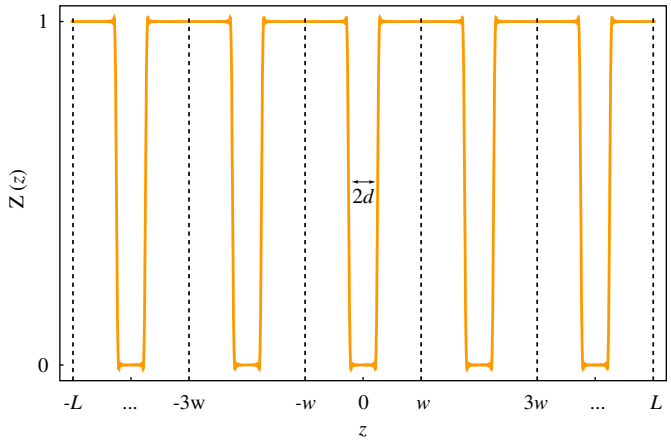


Fig. 3. Schematic representation of $\zeta(z)$ as a function of z and the corresponding Fourier series. The numerical values in the truncate series are $L=600$ nm, $N=5$ and $P=200$.

Author's personal copy

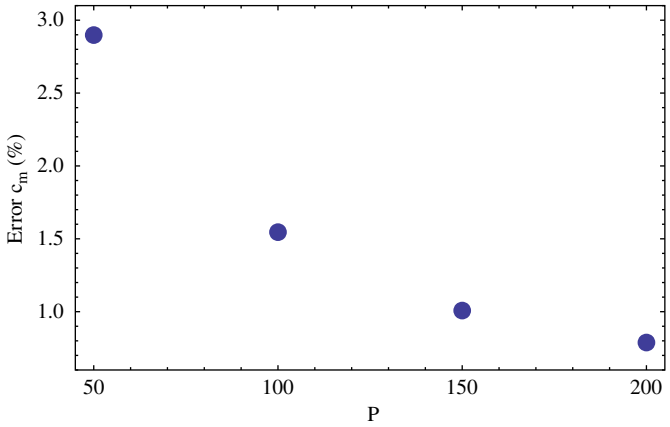


Fig. 4. Relative error between $\tilde{c}_m$ and c_m as a function of P.

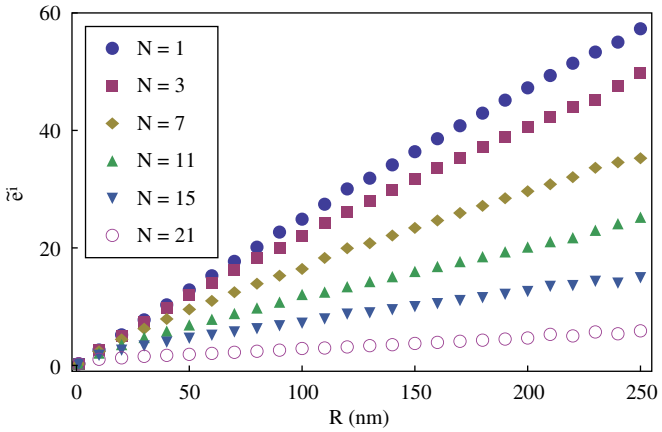


Fig. 5. Normalized self-energy as a function of R for different values of N and $\beta=0.5$, $L=600$ nm.

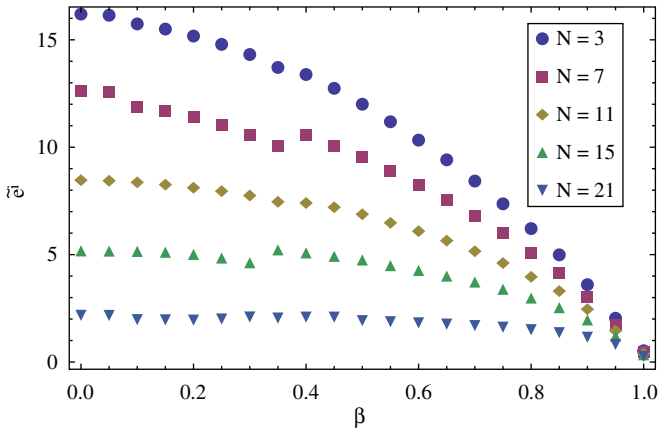


Fig. 6. Normalized self-energy as a function of β for different values of N at $R=50$ nm and $L=600$ nm.

figure we see that when R increases the self-energy increases too. In fact, for each N we find that $\tilde{e}^i$ has a dependence on R of the form $\tilde{e}^i_N(R)=(a+bR)^{1/c}$, where (a,b,c) depend on N and are numerically determined. For example, with $N=11$ one obtains $(a,b,c)=(0.3509,0.2020,1.2225)$. Also, note that when N increases the self-energy strongly decreases, actually $\tilde{e}^i \propto \exp(-\lambda N^2)$.

Fig. 6 shows $\tilde{e}^i$ as a function of the ratio between the external and internal radii, β, for different number of segments, N. Notice that when β increases the self-energy decreases and for $\beta \to 1$ the energies collapse to the same very small value ($e^i \sim 10^{-3}$), regardless of N.

3.2. Interaction energy

Now we focus on the interaction energy, $\tilde{e}^{ij}$, in this multi-segmented system. First, for a fixed distance between the tubes, $D=250$ nm, we examine the dependence on the ratio between the external and internal radii, β, for different number of segments, N, as shown in Fig. 7. One can observe that it decreases when β increases, and when $\beta \to 1$ the energies collapse to almost the same small value ($e^{[ij]} \sim 10^{-3}$), regardless of N, similar to the case of the self-energy.

Let us analyze the dependence of the energy on the length of the tubes. Fig. 8 shows e^{ij} as a function of L for different distances and for a fixed radius. In this figure we obverse that the interaction energy exhibits a maximum at a given length beyond which it monotonically decreases. The position of the maximum depends linearly on the distance, that is $L_m=a+bD_m$ with $a=133$ and $b=0.66$. In addition, for a fixed distance, D, the interaction energy increases with increasing the external radius, R.

Fig. 9 shows the interaction energy as a function of the distance between the tubes, D, for different number of segments, N. We observe that it decreases according to a power law decay

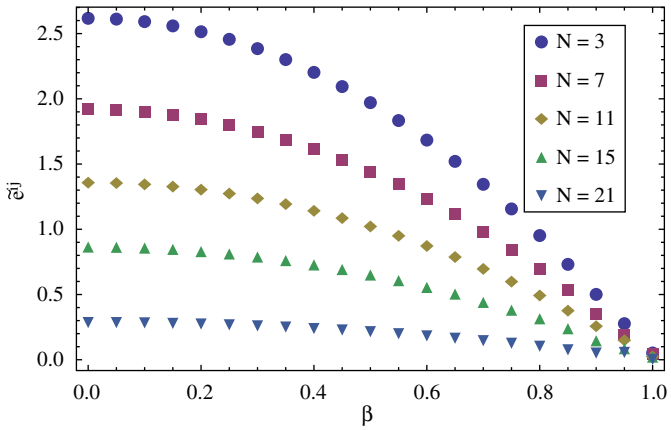


Fig. 7. Normalized interaction energy as a function of β for different values of N at $R=50$ nm and $D=250$ nm and $L=600$ nm.

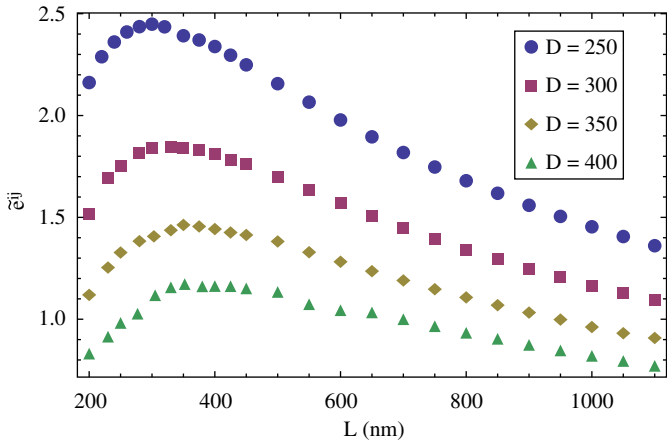


Fig. 8. Normalized interaction energy as a function of L for different values of D at $R=50$ nm, $\beta=0.5$ and $N=3$.

Author's personal copy

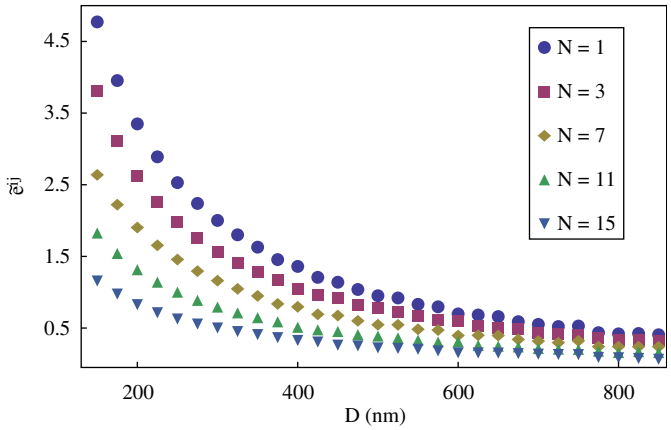


Fig. 9. Normalized interaction energy as a function of D for different values of N at $R=50$ nm, $\beta=0.5$, $L=600$ nm.

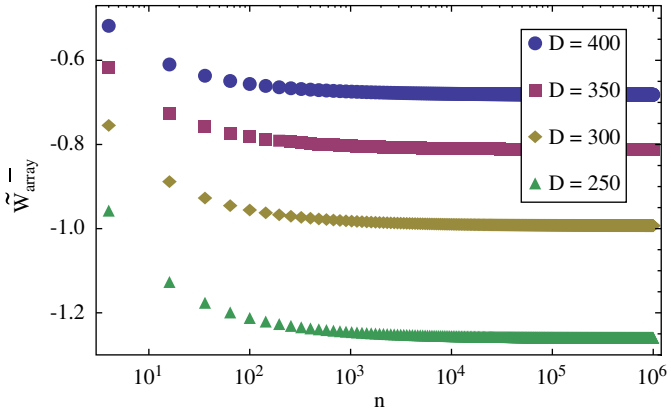


Fig. 10. W^{-}_{array} as a function of n for different D at $N=7$, $R=50$ nm, $\beta=0.5$ and $L=600$ nm.

when the distance increases:

$$\tilde{e}^{ij}_{N}(D)=aD^{-b}, \tag{24}$$

where (a,b) depend of N and are determined numerically. For example, for $N=7$ we get $(a,b)=(1883.9859,1.3044)$ and for $N=15$ we get $(a,b)=(1098.3164,1.3599)$. Also, note that when N increases the interaction energy decreases according to a standard exponential decay law $\tilde{e}^{ij}=a\exp(-bN)$ with $(a,b)=(2.3,0.108)$.

3.3. Square array

With the previous relations for a two particle system, we are now in a position to investigate the effect of the inter-tube magnetostatic coupling in an array. The total energy E_{array} of a square array of $n\times n$ particles can be written as [21]:

$$E^{\pm}_{array}=n^2E_{self}+2n\sum_{p=1}^{n-1}(n-p)(\pm 1)^pE_{int}(pD)$$
$$+2\sum_{p=1}^{n-1}\sum_{q=1}^{n-1}(\pm 1)^{p-q}a_{pq}E_{int}(\Delta_{pq}D), \tag{25}$$

with $\Delta_{pq}=\sqrt{p^2+q^2}$, $a_{pq}=(n-p)(n-q)$ and where the superscripts $+$ $(-)$ refer to the positive or negative value of M_{0j}, respectively, which are related to the magnetic ordering of the array. Actually, the $+$ sign corresponds to a parallel alignment of the magnetization of two elements while the $-$ sign denotes the antiparallel case. We remark that E_{int} in Eq. (25) is the interaction energy between two identical magnetic elements of arbitrary shape. Also, note that an array with a large number of tubes ($n\approx 10^6$), corresponds to a sample close to 0.01 mm^2 that can be experimentally prepared.

Let us analyze our particular case of a multisegmented magnetic structure. In this situation the interaction energy as a function of the distance can be approximated by Eq. (24) for each N. Since the term E_{self} depends only on the geometric characteristics of the tubes, we can define the quantity $W^{\pm}_{array}=(E^{\pm}_{array}-n^2E_{self})/n$ in order to analyze the effect of the interaction between tubes. We consider an array of identical tubes with $R=50$ nm, $\beta=0.5$, $L=600$ nm. Fig. 10 illustrates the behavior of W^{-}_{array} as a function of n for different distances D. We observe that W^{-}_{array} decreases with n and converges to a constant value approximately above $n\sim 10^4$. This value depends on D as shown in Fig. 11. Besides, we observe that for large values of D, the normalized interaction energy of the array tends to zero regardless of N. Finally, let us comment that in the ferromagnetic case, W^{+}_{array} increases with n

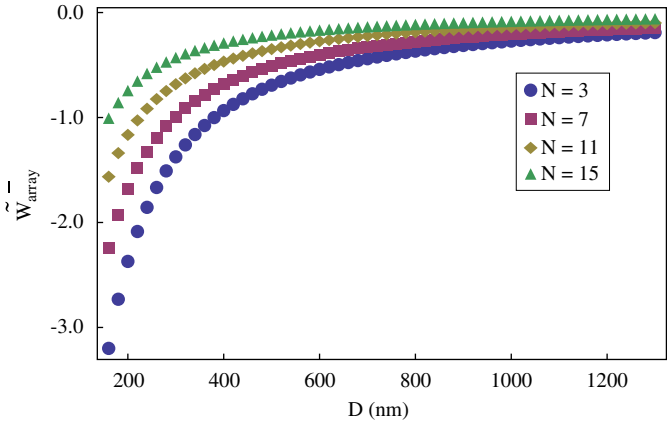


Fig. 11. W^{-}_{array} as a function of D for different values of N at $n=10^4$, $R=50$ nm, $\beta=0.5$ and $L=600$ nm.

and converges to a constant value close to $n\sim 10^7$; and it decreases when D increases.

4. Conclusions

In this paper we have derived general expressions of the self- and magnetostatic interaction energies for two nanostructures with cylindrical shape in a non uniform state where the magnetization along the z-direction is an arbitrary function of z. The results are explicitly given in Eqs. (8) and (12), respectively. When the magnetization is a bound and periodic function of z, we have used the Fourier representation showing that both energies can be reduced to a single integral expression depending on Fourier coefficients. As an example of this technique we analyzed multisegmented nanostructures of the same length but with different number of magnetic regions. We observed that the structures with more segments have lower self- and interaction energies, that tend to zero when the number of segments becomes very large. In the case of a two-particle system we found that the interaction energy decreases according to a power law with the distance between the tubes. Moreover, we studied a square array of multisegmented tubes, finding that for the antiparallel order the interaction energy of the array decreases as a function of the number of particles and for large values of the distance among tubes it tends to zero. Finally, let us remark that this method can be extended to different types of cylindrical particles with distinct magnetization states.

Author's personal copy

Acknowledgments

We thank Harald Pleiner for his critical reading of the manuscript. D.L. acknowledges the partial financial support from Performance Agreement Project UTA/ Mineduc. D.L. and D.A. acknowledge the partial financial support from Millennium Scientific Initiative, *P*10−061−*F*, Basal Program Center for Development of Nanoscience and Nanotechnology (CEDENNA) and Fondecyt thorough grants 11080229 and 1080300. O.J.S. acknowledges the CONICYT PhD program fellowship and the project PIIC2010 USM.

Appendix A. Magnetostatic potential

Here we obtain the magnetostatic potential, $U(\mathbf{r})$, given in Eq. (1) for a magnetic tube with total length $2L$, internal radius r and external radius R when the magnetization is described by $\mathbf{M}(z)=M_0 f(z)\hat{z}$. In order to calculate it, we use the following Green's function representation [46]:

$$\frac{1}{|\mathbf{r}-\mathbf{r}'|}=\sum_{n=-\infty}^{\infty}\exp(in(\phi-\phi'))\times\int_0^{\infty}d\eta F_n(\eta)\exp(-\eta|z_>-z_<|), \quad (A.1)$$

where $F_n(\eta)=J_n(\eta\rho)J_n(\eta\rho')$. Since the potential is the superposition of two parts, $U=U_S+U_V$ (with U_S the surface and U_V the bulk contribution) we can calculate both separately. The superficial contribution can be written as:

$$U_S=\oint_{\mathcal{S}_T}\frac{\mathbf{M}(r')\cdot\hat{\mathbf{z}}'}{\Gamma|\mathbf{r}-\mathbf{r}'|}ds'-\oint_{\mathcal{S}_B}\frac{\mathbf{M}(r')\cdot\hat{\mathbf{z}}'}{\Gamma|\mathbf{r}-\mathbf{r}'|}ds', \quad (A.2)$$

where $\{\mathcal{S}_T,\mathcal{S}_B\}$ denote the top and bottom surface of tube on $z=L$ and $z=-L$, respectively. Using Eq. (A.1) the last expression can be rewritten as:

$$U_S=\frac{M_0}{\Gamma}\sum_{n=-\infty}^{\infty}\int_0^{\infty}d\eta J_n(\eta\rho)g_s(\eta,z)\int_r^R d\rho'\rho' J_n(\eta\rho')\times\int_0^{2\pi}d\phi'\exp(in(\phi-\phi')), \quad (A.3)$$

where

$$g_S(\eta,z)=\epsilon^+\exp(-\eta|z-L|)-\epsilon^-\exp(-\eta|z+L|), \quad (A.4)$$

with $\epsilon^{\pm}=f(\pm L)$ and where $J_n(z)$ is the Bessel function of the first kind. The integration on ϕ' results in $2\pi\delta_{0,n}$ with $\delta_{a,b}$ the Kronecker delta. For $n=0$, the integration on ρ' produce $T(\eta)=RJ_1(\eta R)-rJ_1(\eta r)$. Therefore, Eq. (A.3) is reduced to

$$U_S=\frac{2\pi M_0}{\Gamma}\int_0^{\infty}\frac{d\eta}{\eta}J_0(\eta\rho)T(\eta)g_S(\eta,z). \quad (A.5)$$

The volumetric contribution to the potential is given by

$$U_V=\frac{M_0}{\Gamma}\int_v\frac{1}{|\mathbf{r}-\mathbf{r}'|}\left[\frac{\partial f(z'')}{\partial z''}\right]_{z'}d^3r'. \quad (A.6)$$

Using Eq. (A.1) and after the integration on ρ' and ϕ' we obtain the volumetric component of the potential

$$U_V=\frac{2\pi M_0}{\Gamma}\int_0^{\infty}\frac{d\eta}{\eta}J_0(\eta\rho)T(\eta)g_V(\eta,z), \quad (A.7)$$

where

$$g_V(\eta,z)=\int_{-L}^{L}dz'\exp(-\eta|z-z'|)\left[\frac{\partial f(z'')}{\partial z''}\right]_{z'}. \quad (A.8)$$

Finally, the total magnetostatic potential can be written as:

$$U=\frac{2\pi M_0}{\Gamma}\int_0^{\infty}\frac{d\eta}{\eta}J_0(\eta\rho)T(\eta)g(\eta,z), \quad (A.9)$$

where $g(\eta,z)=g_S(\eta,z)-g_V(\eta,z)$. This is just Eq. (4), used in the main text.

Appendix B. Interaction energy

In this appendix we derive a closed expression for the interaction energy of cylindrical particles in the case of $\mathbf{M}_i(\mathbf{r})=M_{i0}f_i(z)\hat{z}$. The general expression for the energy is given by Eq. (12):

$$e_{int}^{[ij]}=\frac{\pi}{V_i}\int_0^{\infty}d\eta\frac{\omega_{ij}(\eta)}{\eta^2}I_{ij}(\eta), \quad (B.1)$$

with $I_{ij}(\eta)=I_{ij}^S(\eta)+I_{ij}^V(\eta)$, where

$$I_{ij}^S(\eta)=\int_{-L}^{L}dzf_j(z)\left[\frac{\partial}{\partial z'}g_{iS}(\eta,z')\right]_z \quad (B.2)$$

and

$$I_{ij}^V(\eta)=-\int_{-L}^{L}dzf_j(z)\left[\frac{\partial}{\partial z'}g_{iV}(\eta,z')\right]_z. \quad (B.3)$$

The functions g_{iS} and g_{iV} are given in Eqs. (5) and (6), respectively.

Since the magnetization field is null outside the wire, we need to define $f_j(z)$ as

$$f_j(z)=(\Theta(z+L)-\Theta(z-L))\zeta_j(z), \quad (B.4)$$

where $\Theta(\cdot)$ is the Heaviside distribution and $\zeta_j(z)$ is an arbitrary function, but bounded in the range $[-L,L]$. Now, let us assume that $\zeta_j(z)$ is a periodic function. In this case it can be written in the form:

$$\zeta_j(z)=\sum_{m=-\infty}^{\infty}c_m^{(j)}\exp\left(\frac{im\pi}{L}z\right), \quad (B.5)$$

where the coefficients $c_m^{(j)}$ are given by

$$c_m^{(j)}=\frac{1}{2L}\int_{-L}^{L}\zeta_j(z)\exp\left(-\frac{im\pi}{L}z\right)dz. \quad (B.6)$$

Using Eq. (B.5), the expression for I_{ij}^S can be reduced to

$$I_{ij}^S(\eta)=\eta\sum_{m=-\infty}^{\infty}c_m^{(j)}(\epsilon_i^- A_m(\eta,L)-\epsilon_i^+ A_m(\eta,-L)), \quad (B.7)$$

where $\epsilon_i^{\pm}$ becomes $\epsilon_i^{\pm}=\zeta_i(\pm L)$, and where A_m is given by

$$A_m(\eta\pm L)=\int_{-L}^{L}dzS(z\pm L)\exp\left(-\eta|L\pm z|+\frac{im\pi}{L}z\right), \quad (B.8)$$

such that $S(x)$ is the sign function, defined by

$$S(x)=\begin{cases}1 & \text{if } x>0,\\ 0 & \text{if } x=0,\\ -1 & \text{if } x<0.\end{cases} \quad (B.9)$$

The integral given in Eq. (B.8) can be calculated as

$$\int_{-L}^{L}dz\frac{S(z\pm L)}{\exp\left(\eta|L\pm z|-\frac{im\pi}{L}z\right)}=\pm\frac{L(-1)^m\Pi(\eta)}{(\eta L\mp in\pi)}. \quad (B.10)$$

where $\Pi(\eta)=1-\exp(-2\eta L)$. Hence, $I_{ij}^S(\eta)$ can be written in closed form:

$$I_{ij}^S(\eta)=L\eta\Pi(\eta)\sum_{m=-\infty}^{\infty}\frac{(-1)^m c_m^{(j)}(\epsilon_i^-\alpha_m^*+\epsilon_i^+\alpha_m)}{|\alpha_m|^2} \quad (B.11)$$

where $\alpha_m=\eta L-im\pi$ and α_m^* is the complex conjugate of α_m.

By a similar procedure, we can find a compact expression for the volumetric term. Using the Fourier representation of $f_j(z)$ the

Author's personal copy

expression (B.3) becomes

$$I_{ij}^{V}(\eta) = \frac{i\pi\eta}{L} \sum_{n=-\infty}^{\infty} \sum_{m=-\infty}^{\infty} n c_m^{(j)} c_n^{(i)} B_{mn}(\eta, L), \tag{B.12}$$

where the function $B_{mn}(\eta,L)$ is given by

$$B_{mn}(\eta,L) = \int_{-L}^{L} \int_{-L}^{L} \frac{dz dz' S(z-z')}{\exp\left(\eta|z-z'| - i\frac{\pi}{L}(mz+nz')\right)}. \tag{B.13}$$

The last integral can be calculated exactly

$$B_{mn}(\eta,L) = \frac{2\pi i \eta (-1)^{m+n}(n-m)L^3 \Pi(\eta)}{|\alpha_m|^2 |\alpha_n|^2}. \tag{B.14}$$

Consequently, I_{ij}^{V} can be written as

$$I_{ij}^{V}(\eta) = \Lambda(\eta) \sum_{m,n=-\infty}^{\infty} \frac{(-1)^{m+n} n(m-n) c_m^{(j)} c_n^{(i)}}{|\alpha_m|^2 |\alpha_n|^2}, \tag{B.15}$$

where $\Lambda(\eta) = 2(\pi\eta L)^2 \Pi(\eta)$. We remark that, Eqs. (B.11) and (B.15) allow the interaction energy, Eq. (B.1), to be expressed a single integral.

References

[1] A. Thiaville, J. Miltat, Science 284 (1999) 5422.
[2] T. Gerrits, H. van den Berg, J. Hohlfeld, L. Bar, T. Rasing, Nature 418 (2002) 509.
[3] S. Tehrani, J.M. Slaughter, M. DeHerrera, B. Engel, N.D. Rizzo, J. Salter, J. Durlam, R.W. Dave, J. Janesky, B. Butcher, K. Smith, G. Grynkewich, Proceedings of the IEEE 91 (2003) 703.
[4] M.R. Freeman, B.C. Choi, Science 294 (2001) 1484.
[5] S.D. Bader, Reviews of Modern Physics 78 (2006) 1.
[6] J. Martin, J. Nogues, K. Liu, J.L. Vicent, I.K. Schuller, Journal of Magnetism and Magnetic Materials 256 (2003) 449.
[7] C. Ross, Annual Review of Materials Research 31 (2001) 203.
[8] K. Nielsch, R.B. Wehrspohn, J. Barthel, J. Kirschner, S.F. Fischer, H. Kronmuller, T. Schweinbock, D. Weiss, U. Gosele, Journal of Magnetism and Magnetic Materials 291 (2002) 234.
[9] K. Nielsch, R.B. Wehrspohn, J. Barthel, J. Kirschner, U. Gosele, S.F. Fischer, H. Kronmuller, Applied Physics Letters 79 (2001) 1360.
[10] M. Vazquez, K. Nielsch, P. Vargas, J. Velazquez, D. Navas, K. Pirota, M. Hernandez-Velez, E. Vogel, J. Cartes, R.B. Wehrspohn, U. Gosele, Physica B 343 (2004) 395.
[11] M. Vazquez, K. Pirota, J. Torrejon, D. Navas, M. Hernandez-Velez, Journal of Magnetism and Magnetic Materials 294 (2005) 174.
[12] R. Skomski, H. Zeng, M. Zheng, D.J. Sellmyer, Physical Review B 62 (2000) 3900.
[13] R. Varga, K.L. Garcia, M. Vazquez, P. Vojtanik, Physical Review Letters 94 (2005) 017201.
[14] L.C. Sampaio, E.H. Sinnecker, G. Cernicchiaro, M. Knobel, M. Vazquez, J. Velazquez, Physical Review B 61 (2000) 8976.
[15] M. Knobel, L.C. Sampaio, E. Sinnecker, P. Vargas, D. Altbir, Journal of Magnetism and Magnetic Materials 249 (2002) 60.
[16] Q. Zhan, J. Gao, Y. Liang, N. Di, Z. Cheng, Physical Review B 72 (2005) 024428.
[17] J. Velazquez, M. Vazquez, Journal of Magnetism and Magnetic Materials 249 (2002) 89.
[18] J. Velazquez, K.R. Pirota, M. Vazquez, IEEE Transactions on Magnetics 39 (2003) 3049.
[19] M. Beleggia, S. Tandon, Y. Zhu, M. De Graef, Journal of Magnetism and Magnetic Materials 278 (2004) 270.
[20] M. Beleggia, M. De Graef, Journal of Magnetism and Magnetic Materials 285 (2005) L1.
[21] D. Laroze, J. Escrig, P. Landeros, D. Altbir, M. Vazquez, P. Vargas, Nanotechnology 18 (2007) 415708.
[22] R. Piccin, D. Laroze, M. Knobel, P. Vargas, M. Vazquez, Europhysics Letters 78 (2007) 67004.
[23] R. Hertel, Journal of Applied Physics 90 (2001) 5752.
[24] L. Clime, P. Ciureanu, A. Yelon, Journal of Magnetism and Magnetic Materials 297 (2006) 60.
[25] M. Bahiana, F.S. Amaral, S. Allende, D. Altbir, Physical Review B 74 (2006) 174412.
[26] D. Laroze, S.A. Baranov, P. Vargas, M. Vazquez, Physica Status Solidi (c (2007) 4170;
S.A. Baranov, D. Laroze, P. Vargas, M. Vazquez, Physica B 372 (2006) 320;
D. Laroze, P. Vargas, D. Altbir, M. Vazquez, Brazilian Journal of Physics 36 (2006) 908;
S.A. Baranov, D. Laroze, P. Vargas, M. Vazquez, Physica B 372 (2006) 324.
[27] E.V. Tartakovskaya, M. Pardavi-Horvath, M. Vazquez, Journal of Magnetism and Magnetic Materials 322 (2010) 743.
[28] E.V. Tartakovskaya, A. Vovk, V. Golub, Physics Status Solidi A – Applied Materials 205 (2008) 1787.
[29] C.A. Ramos, E.V. Brigneti, M. Vazquez, Physica B 354 (2004) 195.
[30] H. Lee, S. Kim, Y. Chang, K.H. Yoo, J. Lee, Journal of Magnetism 14 (2009) 1.
[31] K. Nielsch, F.J. Castano, C.A. Ross, R. Krishnan, Journal of Applied Physics 98 (2005) 034318.
[32] K. Nielsch, F.J. Castano, S. Matthias, W. Lee, C.A. Ross, Advanced Engineering Materials 7 (2005) 217.
[33] M. Daub, M. Knez, U. Gosele, K. Nielsch, Journal of Applied Physics 101 (2007) 09J111.
[34] Z.K. Wang, H.S. Lim, H.Y. Liu, S.C. Ng, M.H. Kuok, L.L. Tay, D.J. Lockwood, M.G. Cottam, K.L. Hobbs, P.R. Larson, J.C. Keay, G.D. Lian, M.B. Johnson, Physical Review Letters 94 (2005) 137208.
[35] J. Escrig, P. Landeros, D. Altbir, E.E. Vogel, P. Vargas, Journal of Magnetism and Magnetic Materials 308 (2007) 233.
[36] V. Lehmann, Nature Materials 1 (2002) 12.
[37] S.R. Nicewarner-Peña, F.R. Griffith, B.D. Reiss, L. He, D.J. Peña, I.D. Walton, R. Cromer, C.D. Keating, M.J. Natan, Science 294 (2001) 137.
[38] W. Lee, R. Scholz, K. Nielsch, U. Güsele, Angewandte Chemie International Edition 44 (2005) 6050.
[39] S. Jun Son, J. Reichel, B. He, M. Schuchman, S. Bok Lee, Journal of American Chemical Society 127 (2005) 7316.
[40] M. Albrecht, G. Hu, A. Moser, O. Hellwig, B.D. Terris, Journal of Applied Physics 97 (2005) 103910.
[41] R.L. Stoermer, K.B. Cederquist, S.K. McFarland, M.Y. Sha, S.G. Penn, C.D. Keating, Journal of American Chemical Society 128 (2006) 16892.
[42] S.J. Hurst, E.K. Payne, L.D. Qin, C.A. Mirkin, Angewandte Chemie International Edition 45 (2006) 2672.
[43] S. Mukherjee, X.P. Li, F. Gao, Z. Gu, Electrochemical Solid-State Letters 10 (2007) C63.
[44] J. Escrig, P. Landeros, D. Altbir, M. Bahiana, J. d'Albuquerque e Castro, Applied Physics Letters 89 (2006) 132501.
[45] B. Leighton, O.J. Suarez, P. Landeros, J. Escrig, Nanotechnology 20 (2009) 385703.
[46] J.D. Jackson, Classical Electrodynamics, Third ed., John Wiley Sons, Inc., USA, 1999.
[47] A. Aharoni, Introduction to the Theory of Ferromagnetism, Oxford Science Publications, New York, 2000.
[48] S. Tandon, M. Beleggia, Y. Zhu, M. De Graef, Journal of Magnetism and Magnetic Materials 271 (2004) 9.
[49] D. Vakoun, M. Beleggia, L. Heller, P. Sittner, Journal of Magnetism and Magnetic Materials 321 (2009) 3758.
[50] M. Beleggia, S. Tandon, Y. Zhu, M. De Graef, Journal of Magnetism and Magnetic Materials 278 (2004) 270.
[51] P. Landeros, J. Escrig, D. Altbir, D. Laroze, J. d'Albuquerque e Castro, P. Vargas, Physical Review B 71 (2005) 094435.
[52] D. Vokoun, M. Beleggia, L. Heller, P. Sittner, Journal of Magnetism and Magnetic Materials 321 (2009) 3758.
[53] D. Vokoun, G. Tomassetti, M. Beleggia, I. Stachiv, Journal of Magnetism and Magnetic Materials 323 (2011) 55.
[54] O.J. Suarez, P. Vargas, E.E. Vogel, Journal of Magnetism and Magnetic Materials 321 (2009) 3658.
[55] J. Escrig, P. Landeros, D. Altbir, M. Bahiana, J. d'Albuquerque e Castro, Applied Physics Letters 89 (2006) 132501.
[56] E. Feldtkeller, H. Thomas, Physik der Kondensierten Materie 4 (1965).
[57] P.O. Jubert, R. Allenspach, Physical Review B 70 (2004) 144402.
[58] I.S. Gradshteyn, I.M. Ryzhik, A. Jeffrey, D. Zwillinger, Table of Integrals, Series, and Products, Academic Press, 2000.
[59] H. Weber, G. Arfken, Essential Mathematical Methods for Physicists, Academic Press, 1985.
[60] R.W. Hamming, Numerical Methods for Scientists and Engineers, 2nd ed., Dover, New York, 1986.